BMBF Verbundprojekt

Reports on DKRZ Resources 2021

PalMod – Paleo Modelling Initiative Phase II:

From the Last Interglacial to the Anthropocene –
Modelling a Complete Glacial Cycle

Principal Investigators: Mojib Latif[1],
Tatiana Ilyina[2],
Michael Schulz[3]

(1) GEOMAR, Kiel (to whom correspondence should be sent)
(2) MPI-M, Hamburg
(3) MARUM, Bremen

Executive Summary

The report summarizes the individual reports of the projects associated to the consortium project **PalMod Phase II** and covers the time period from 2021-01-01 to 2021-07-31 unless stated otherwise.

Table of Contents

Summary

As 2020, 2021 was a difficult year for the project due to the COVID19 pandemic situation. There were still some impacts on the progress of PalMod due closed childcare facilities for several months, challenges of working from home with less efficient communication between colleagues and last but not least some project members on parental leave.

As a consequence, some of the WGs were handicapped and not able to use the granted resources as planned. Nevertheless, because we had the permission to shift the computing time between the PalMod accounts we were able to provide groups with resources that could not be used otherwise and were able to complete some tasks faster.

As an interim result (August 2021) from the computing time granted to the PalMod consortia less then 1.5 % had to be cut after Q1 and Q2.

But the archiving of the data is behind the schedule. The reason is, that the main PalMod highlight experiments are performed yet and before we can store the results in the archive the validation procedures have to be finished.

Finally, the results will be made available in the next months and stored together with the metadata. For details, please see the Data Management Plan (DMP) attached to the resource application.

Block Grant for PalMod Consortia	Granted	Used by end of July	Remarks
Computing time. [n*h]	2.144.856	1.277.098	> 1.5% cut in Q1 and Q2
/work [TiB]	2.221	2.087	
HPSS /arch [TB]	1.605	594	
/doku [TB]	573	-	

1. Project 989 / WG1

Project title: PalMod WG1 - The Physical System
Project leader: G. Lohmann (AWI), U. Mikolajewicz (MPI-M)
Sublead: G.Lohmann (AWI), V.Klemann (GFZ), U.Mikolajewicz (MPI-M), M.Prange (MARUM), (MPI-M), R.Winkelmann (PIK), T.Martin (GEOMAR)
Allocation period: 01.01.2021 – 31.07.2021

1.1 Report on resources used in 2021

At the MPI-Met, we performed an ensemble of fully synchronously-coupled simulations of the last deglaciation with the MPI-ESM-CR-PISM-VILMA model setup. This model setup also includes an interactive iceberg module. For the northern hemisphere, the volume evolution from the Last Glacial Maximum (LGM, ca. 21 ka BP) to present-day matches well with the ICE6G and Glac1D ice-sheet reconstructions (Fig. 1a). In the latter part of the deglaciation, ice loss rates are a little too small in comparison to the reconstructions, resulting in higher present-day ice volume for the northern hemisphere. We have also made progress in tuning the Antarctic ice sheet. Most of the simulations model an Antarctic ice sheet that is at the continental shelf edge at the LGM. However, our simulations reveal that the parameter range, in which the ice sheet advances to the continental shelf edge at LGM and retreats to its present-day position, is very narrow (Fig. 1b). In addition, small changes in the deglaciation timing of the northern hemisphere also affect the retreat and advance of the Antarctic ice sheet. Our recent progress of the southern hemisphere tuning was also hampered by the bug discovered in the atmosphere-ocean coupling of MPI-ESM at the start of 2021. This meant that we had to re-tune the southern and northern hemisphere.

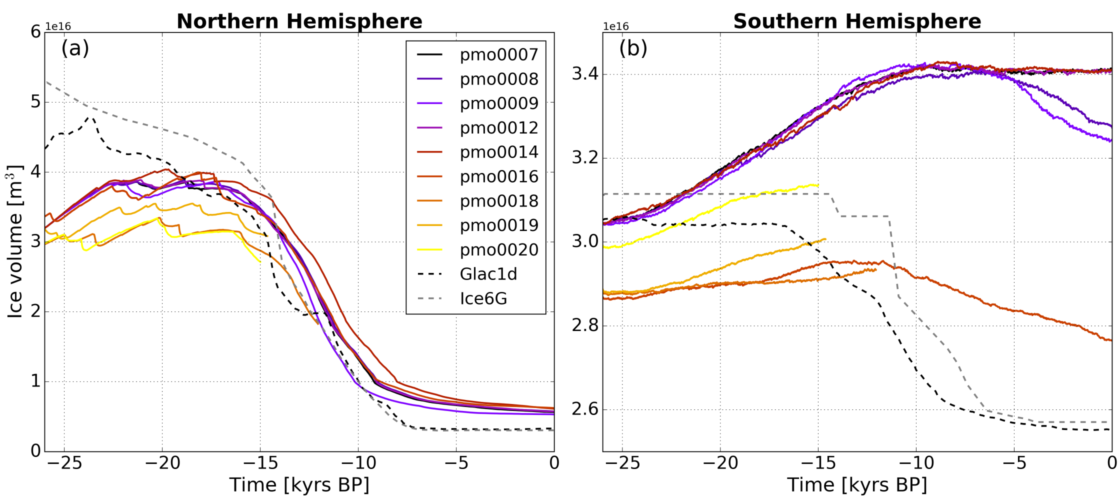

Figure 1: Ice volume evolution of fully-synchronously coupled deglaciation ensemble (solid lines) and ice sheet reconstructions (dashed lines) for the northern (a) and southern hemisphere (b).

All ensemble members show multiple events during which the Atlantic meridional overturning circulation (AMOC) is either considerably weakened or shuts down entirely (Fig. 2b). While the timing and magnitude of these events varies across the ensemble members, most of these events exhibit a clear global cooling signal (Fig. 2a). The AMOC shutdowns are closely interlinked with ice-sheet surge events from the Laurentide as well as the Fennoscandian ice sheet. During the surge events large amounts of ice are discharged into the ocean, resulting in a significant increase in global freshwater uptake (Fig. 2c). The magnitude of the simulated surge events also roughly corresponds to what is known from observations.

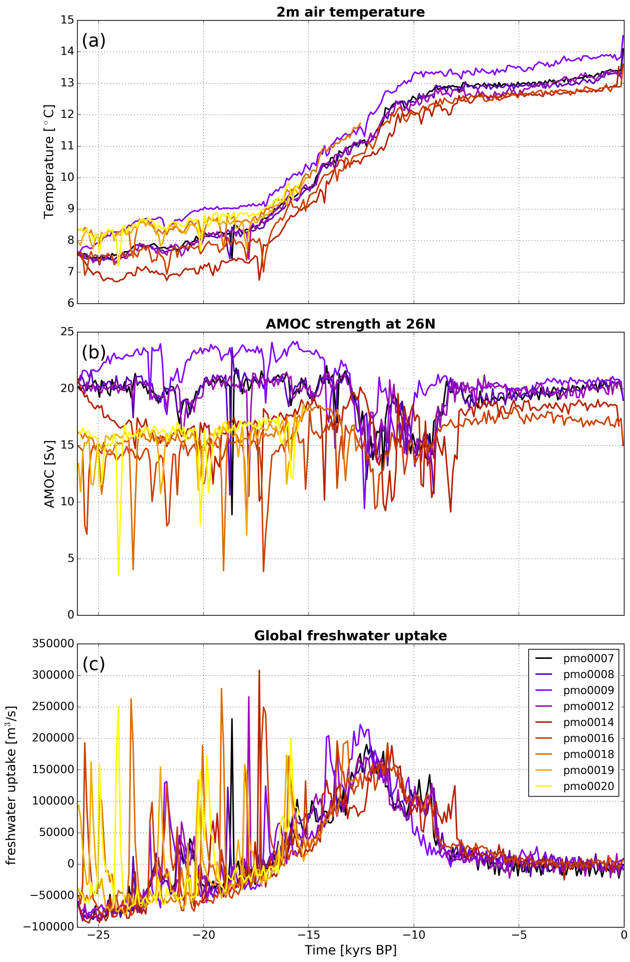

Figure 2: Time evolution of (a) 2m air temperature, (b) AMOC strength at 26°N, and (c) global freshwater uptake for the fully-synchronously coupled deglaciation ensemble.

In addition to our deglaciation simulations, we also performed several asynchronously coupled simulations of Marine Isotope Stage (MIS) 3 between 65-30 ka BP with the MPI-ESM-CR-PISM-VILMA model setup. In these MIS3 simulations, and in many tuning simulations of the last deglaciation, the occurrence of Heinrich-type ice-sheet surges from the Laurentide ice sheet often appeared synchronized (Fig. 3). We have started to investigate in a simpler model setup what controls this apparent synchronicity, using PISM-VILMA together with forcing from fully-coupled MIS3 simulations. Preliminary findings indicate that in our model simulations the synchronicity between the ice-sheet surges from the Laurentide ice sheet are most likely influenced by climate forcing.

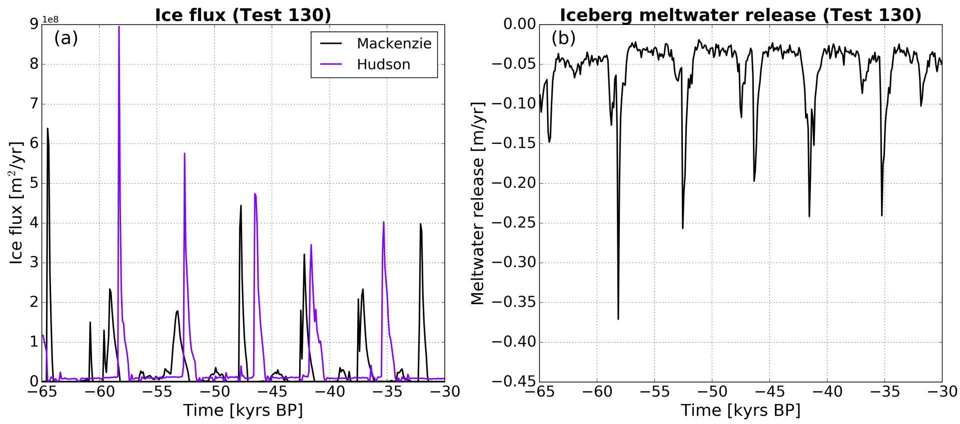

Figure 3: (a) Ice flux time series for Hudson (purple) and Mackenzie area (black). (b) shows corresponding iceberg meltwater flux at a point location (38.4°N, 26°E) in the Atlantic Ocean*.*

The GFZ (WP1.4-TP1) utilized the VIscoelastic Lithosphere and MAntle model VILMA to reconstruct relative sea-level changes and solid earth deformation in PalMod. In 2021, Hereon provided computing time for the GFZ.

To test the timing of the Malacca strait opening, we reconstructed the relative sea-level change during the last deglaciation with an ensemble of Earth structures using VILMA, where influences of glacial-isostatic adjustment (GIA) and hydro-isostatic adjustment (HIA) on the relative sea-level are considered. We reconstruct the relative sea-level curves at the location of 1.2ºN/103.7ºE in the Malacca Strait (Fig. 4, 5). According to a present-day water depth of 30 m, the strait started to open between ~12.3 and ~11.4 ka BP (Shi et al. in prep.).

In addition to the existing 3D model ensemble with a set of 3D Earth structures and three ice histories (Bagge et al. in revision), we started to extend our VILMA standalone models by applying further ice histories which are derived from the MPI-PISM ice history for the northern hemisphere and from the PIK-PISM ice history for the southern hemisphere under usage of different Earth structures.

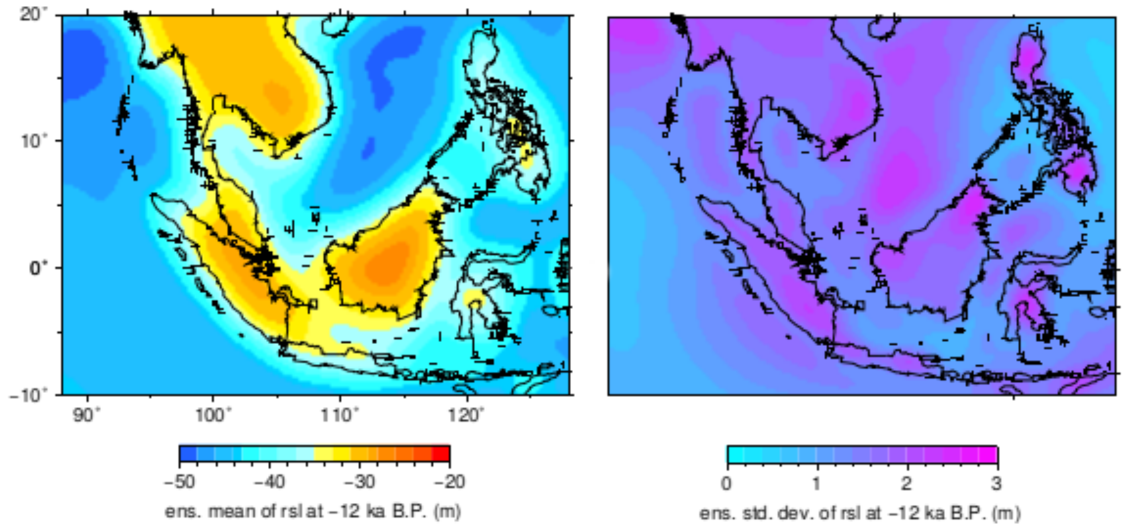

Figure 4: Spatial distribution of relative sea-level in the Malacca strait region. Ensemble mean (left), and ensemble standard deviation (right) reconstructed with the GIA model VILMA at 12 ka B.P. Ensemble members differ in earth structure variability. The relative sea-level in the Malacca strait ranges between ~25-35 m. The standard deviation amounts less than 2 m, and the range between ensemble maximum and minimum varies by ~10 m (Shi et al. in prep.).

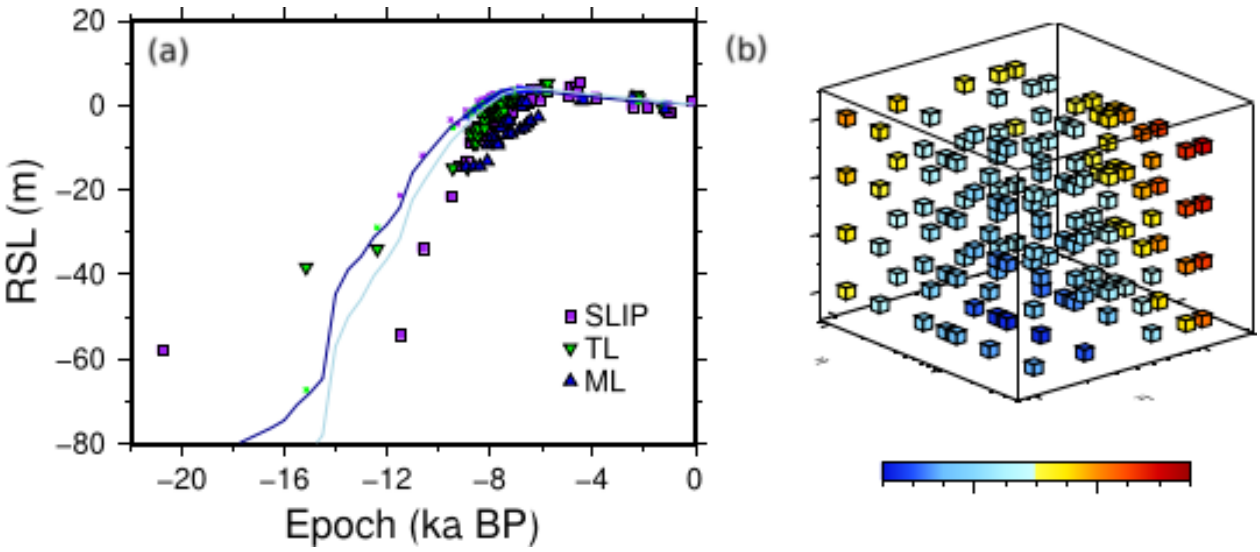

Figure 5: (a) Relative sea-level curve for ensemble minimum (light blue) and ensemble maximum (dark blue) at location 1.2ºN/103.7ºE. The GIA model ensemble is based on ICE-6G and a range of Earth structures regarding lithosphere thickness and viscosity in upper and lower mantle. Sea-level data are divided in terrestrial limiting data (TL, green), marine limiting data (ML, blue) and sea-level index points (SLIP, purple) (Shi et al. in prep.). (b) Variability of flooding time within the GIA model ensemble at location 1.2°N/103.7°E and assuming a present-day depth of 30 m. The ensemble member with a high lithospheric thickness of 120 km, an upper mantle viscosity of 1 x 10^{21}Pa s and a lower mantle viscosity of 5 x 10^{22}Pa s has the highest paleotopography and therefore the reconstructed opening of the Strait of Singapore (flooding time) was the latest at ~11.4 ka B.P. The earliest strait opening is reconstructed ~12.3 ka B.P. (lowest paleotopography) for the ensemble member with a thin lithospheric thickness of 60 km, an upper mantle viscosity of 2 x 10^{20} Pa s and a lower mantle viscosity of 2 x 10^{22} Pa s (Shi et al. in prep).

The AWI has continued development of the AWI-ESM2 model. In this phase of the project the AWI-ESM is subject to implementation of various processes and components. This work is related to substantial workload and complex tasks. The FESOM2 has been updated to the newest version with z * coordinates, providing the infrastructure that is necessary to consider ice cavities in the coupled long term transient climate – ice sheet simulations. Some model developments that have been achieved in the framework of PalMod2 (for example the iceberg module) have been upgraded accordingly. The diurnal Energy Balance Model (dEBM), that has shown to improve the simulation of ice sheets in the Northern Hemisphere, has been published by Krebs-Kanzow et al. (2021). For ice sheet and ocean dynamics in a coupled setup, consideration of the impact of lakes is important. Abrupt change of the state of glacial lakes may lead to significant freshwater release into the oceans. With the FESOM as a multiresolution model in the global domain, the impact of different routes of freshwater release on ocean dynamics can be realistically considered in climate simulations (Lohmann et al., 2020). A sensitivity study by Sun et al. (2020) has shown that ocean circulation is indeed sensitive to this process. A respective module by Hink et al. (2020a,b) is currently being integrated into the most recent AWI-ESM2 modelling framework, that does not only consider updates to the model components, but also to the modular infrastructure for coupled Earth System Modelling (ESM; Barbi et al., 2021).

In PalMod-II-1-1-TP1 the AWI-ESM2 and the PISM have been used to study the coupled ice sheet – climate system for various orbital configurations and average greenhouse gas concentrations in the glacial/interglacial phase space. Niu et al. (2021) have presented a discussion of the oscillatory behavior of the Cordilleran Ice Sheet, that reaches the ocean during glacial state, collapses, and thereafter returns to its initial state as a result of internal ice sheet – climate interactions (Fig. 6). These internal oscillations of ice sheets may occur independently of variations in insolation, have been recently reported in geologic records (Maier et al., 2018), and may be an explanation of Heinrich-type oscillations found during MIS 3 and MIS2 in the Pacific Ocean.

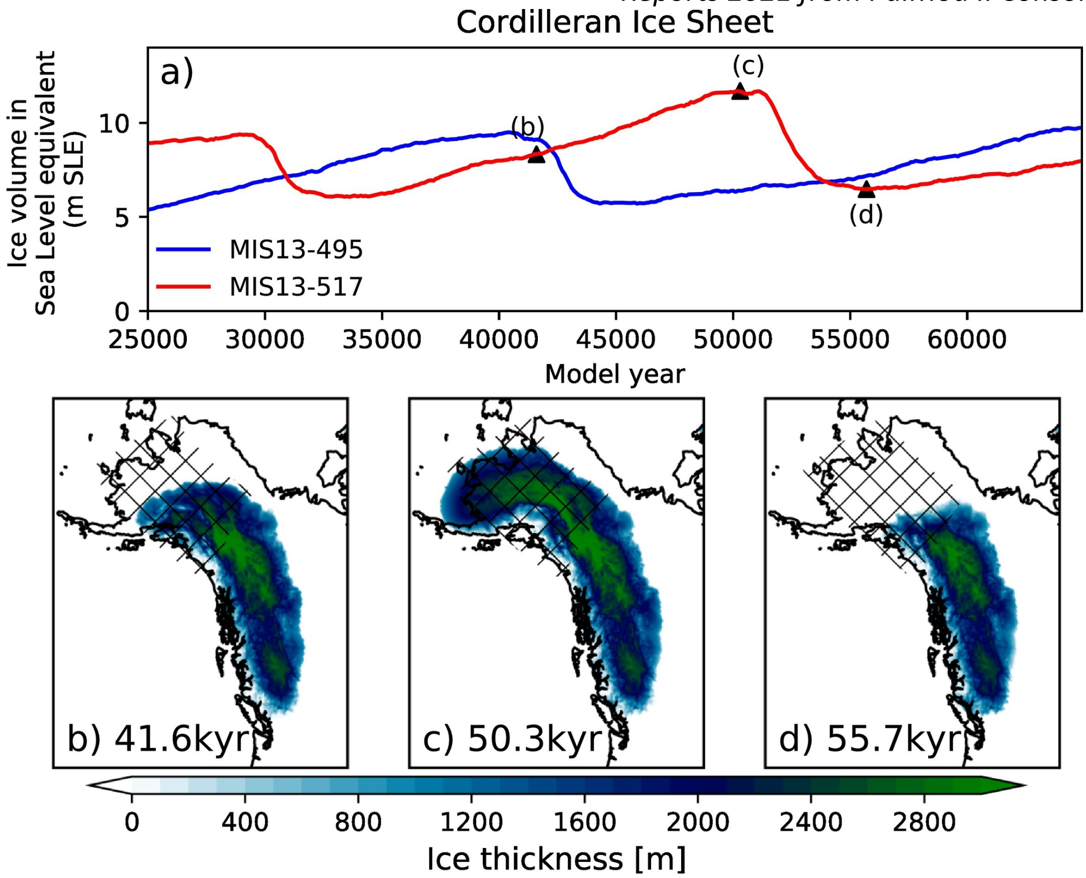

Figure 6: Oscillatory behavior of ice sheet volume of the Cordilleran Ice Sheet over time at fixed climate forcing. Triangles in (a) depict the time for different configurations of the ice sheet that are shown in (b-d).

In PalMod-II-1-3-TP1, AWI investigated transient inception with AWI-ESM2. We have performed sensitivity studies testing the impact of greenhouse gases and orbital parameters on glacial inception for the time slice of 115 ka BP, both with the coupled climate – ice sheet configuration of AWI-ESM2 and in a standalone ice sheet modelling configuration. Our results suggest low sensitivity of glacial inception in the coupled model regarding greenhouse gas concentration. Despite strongly reduced near surface temperatures and increased winter precipitation (Fig. 7) there is no development of perennial snow cover in the regions of interest if climate conditions are considered for a modern topography. Buildup of ice mass only occurs after introducing initial ice sheet nuclei (Fig. 8). This highlights the need for further studies regarding the impact of uncertainties in ice sheet nuclei on the glaciation history. We will follow this lead in the framework of T1.3-5 in the follow up proposal (please consider the request document for the upcoming allocation period).

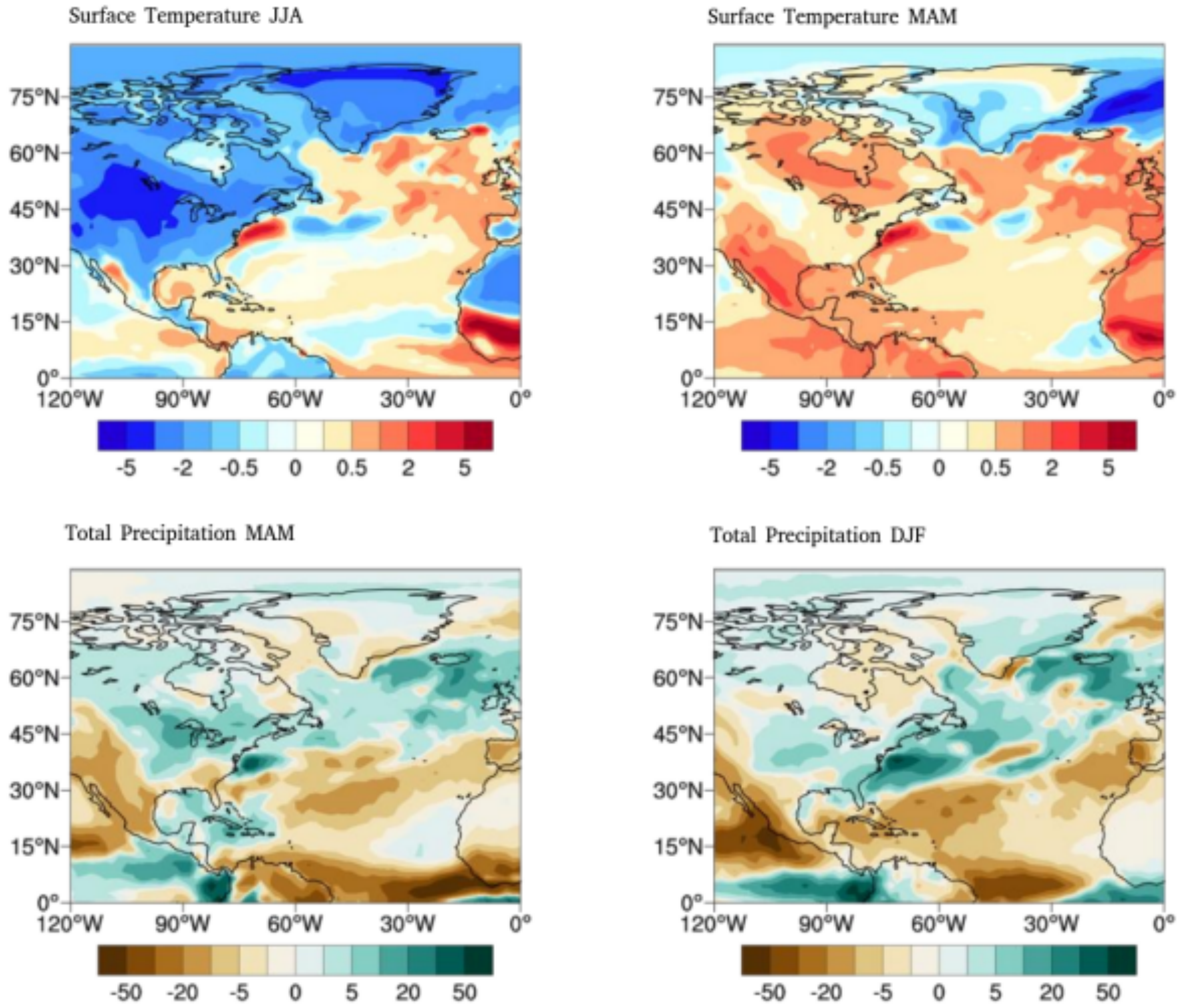

Figure 7: Anomalies, 115 ka wrt. preindustrial, of surface temperature for summer and spring (top), and of precipitation for spring and winter (bottom) after an integration time of 20,000 years

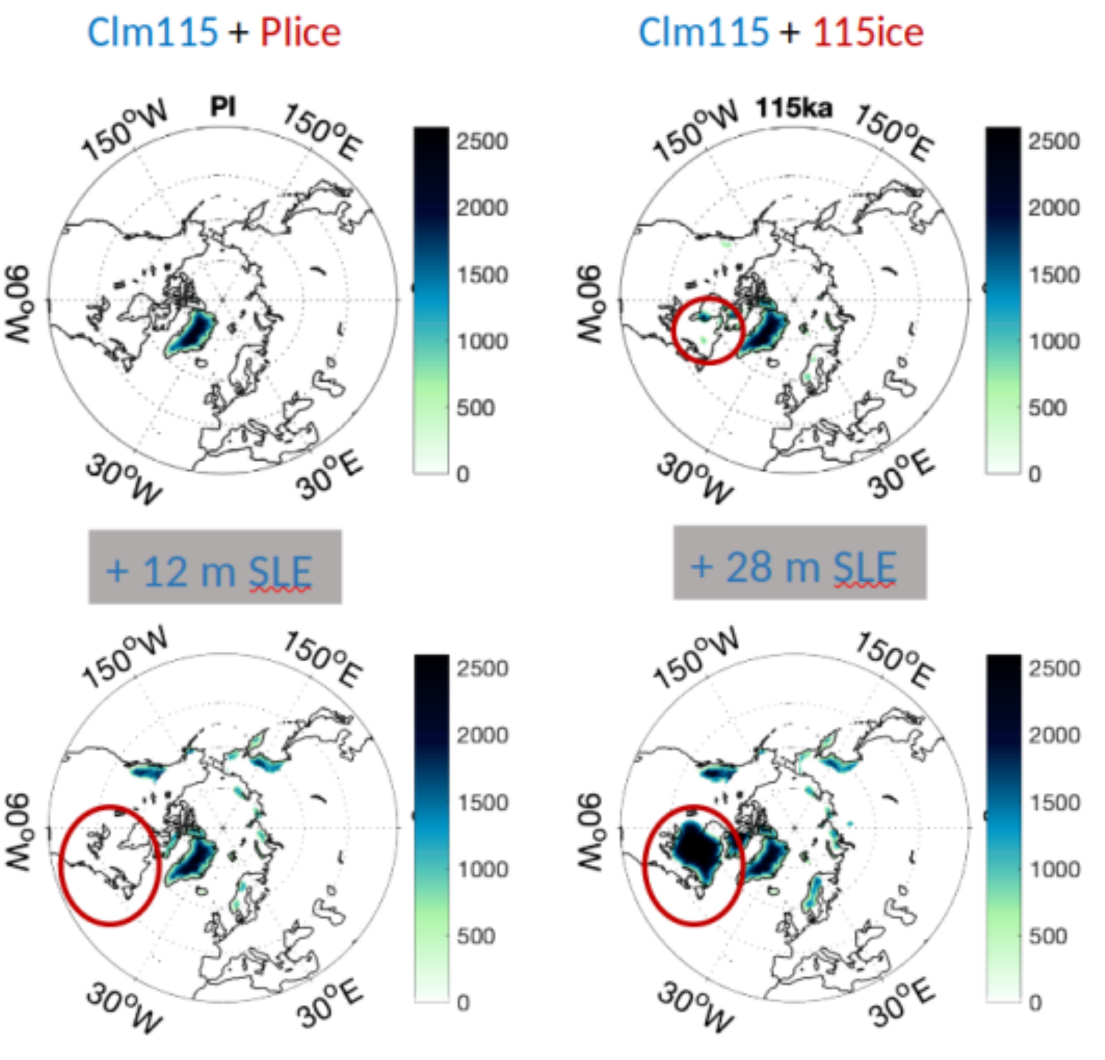

Figure 8: Thickness of the ice sheets simulated with 115 ka climatic conditions at initialization (top) and after integration over 20,000 years (bottom) without (left) and with (right) ice sheet nuclei in northern America.

In PalMod-II-1-2-TP1 the AWI has investigated the mean climate state and major teleconnections for preindustrial, LGM (21 ka), and MIS3 based on AWI-ESM2. The work has considered the reconstruction of global ice sheets by Gowan (2019) and Gowan et al. (2021). For 57.5 ka and 45 ka BP the model has been used to simulate temperature anomalies with respect to preindustrial conditions. The results suggest appreciably cooler annual mean conditions across Eurasia, MIS3 Laurentide Ice Sheet, Barents Sea, and parts of the Nordic Seas, where sea ice extends further than for the preindustrial. Based on an analysis of surface temperature teleconnections we conclude that modern teleconnections are not suitable for the reconstruction of glacial climate (Fig. 9). On the other hand, strong glacial teleconnections imply that a limited number of proxy data sets may be sufficient to fully capture the glacial climate state.

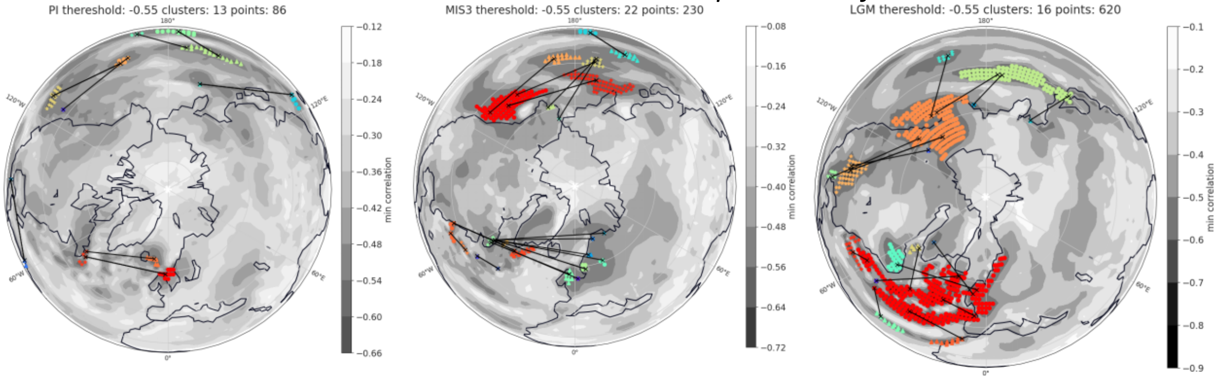

Figure 9: Comparison of the strength of teleconnections of surface temperature for simulated PI (left), MIS3 (middle), and LGM (right) climate states. The minimum correlation of any grid cell with any other grid cell is shown in grayscale. Strongest centers of teleconnections (i.e., the local minima) are shown in colors, the strongest teleconnections between the various regions are indicated by lines.

1.2 Publications and References

Bagge, M., Klemann, V., Steinberger, B., Latinović, M., and Thomas, M.: Glacial-isostatic adjustment models using geodynamically constrained 3D Earth structures, Geochem., Geophys., Geosys, in revision.

Barbi, D., Wieters, N., Gierz, P., Andrés-Martínez, M., Ural, D., Chegini, F., Khosravi, S., and Cristini, L.: ESM-Tools version 5.0: a modular infrastructure for stand-alone and coupled Earth system modelling (ESM), Geosci. Model Dev., 14, 4051–4067, https://doi.org/10.5194/gmd-14-4051-2021, 2021.

Gowan, E. J: Global ice sheet reconstruction for the past 80000 years, PANGAEA, https://doi.org/10.1594/PANGAEA.905800, 2019.

Gowan, E. J., Zhang, X., Khosravi, S., Rovere, A., Stocchi, P., Hughes, A. L. C., Gyllencreutz, R., Mangerud, J., Svendsen, J.-I., and Lohmann G.: A new global ice sheet reconstruction for the past 80 000 years, Nature Communications, DOI: 10.1038/s41467-021-21469-w, 2021.

Hinck, S., Gowan, E. J., and Lohmann, G.: LakeCC: a tool for efficiently identifying lake basins with application to paleo-geographic reconstructions of North America, Journal of Quaternary Science, 35 (3), 422-432, DOI:10.1002/jqs.3182, 2020a.

Hinck, S., Gowan, E. J., Zhang, X., and Lohmann, G.: PISM-LakeCC: Implementing an adaptive proglacial lake boundary into an ice sheet model, The Cryosphere Discuss., in review, https://doi.org/10.5194/tc-2020-353, 2020.

Krebs-Kanzow, U., Gierz, P., Rodehacke, C. B., Xu, S., Yang, H., and Lohmann, G.: The diurnal Energy Balance Model (dEBM): a convenient surface mass balance solution for ice sheets in Earth system modeling, The Cryosphere, 15, 2295–2313, 2021.

L*ohmann, G., Butzin, M., Eissner, N., Shi, X., and Stepanek, C*.: Abrupt climate and weather changes across time scales, Paleoceanogr. and Paleoclimatol., 35, e2019PA003782, https://doi.org/10.1029/2019PA003782, 2020. Special Section AGU Grand Challenges in the Earth and Space Sciences.

Maier, E., Zhang, X., Abelmann, A., Gersonde, R., Mulitza, S., Werner, M., Méheust, M., Ren, J., Chapligin, B., Meyer, H., Stein, R., Tiedemann, R., and Lohmann, G.: North Pacific freshwater events linked to glacial ocean circulation changes, Nature, 559, 241–245, doi:10.1038/s41586-018-0276-y, 2018.

Niu, L., Lohmann, G., Gierz, P., Gowan, E.J., and Knorr, G.: Coupled climate-ice sheet modelling of MIS-13 reveals a sensitive Cordilleran Ice Sheet, Global and Planetary Change, 103474, doi:10.1016/j.gloplacha.2021.103474, 2021

Sun, Y, Knorr, G., Zhang, X., Tarasov, L., Barker, S., Werner, M., and Lohmann, G.: Ice Sheet Decline and Rising Atmospheric CO2 Control AMOC Sensitivity to Deglacial Meltwater Discharge, Global and Planetary Change, submitted, 2020.

Shi X.F., Liu S.F., Bagge M., Gowan, E.J., Klemann V., Cao P., Zhang X. Opening of the Malacca Strait at the start of the Holocene. In preparation.

2. Project 1030 / WG2

Project title: PalMod WG2 - Biogeochemistry
Project lead: V.Brovkin (MPI-M), P. Köhler (AWI)
Subproject lead: P.Köhler (AWI), M.Claussen (MPI-M), B.Schneider (CAU Kiel), T.Ilyina (MPI-M), T.Kleinen (MPI-M), B.Steil (MPI-C), A.Paul(MARUM)
Allocation period: 01.01.2021 – 31.07.2021

2.1 Report on resources used in 2021

Preamble

2021 was a difficult year due to the COVID19 pandemic. The main impact on PalMod and thus project bm1030 was that some childcare facilities were closed for several months, severely impacting the ability of project members to work. Furthermore, the challenges of working from home and the less efficient communication between colleagues caused further delays.

WP2.1 (MPI-M)
We only used a fraction (about 80%) of the allocated computing time for the following reasons. 1) The transient deglaciation simulations, which constitute almost 60% of the planned simulations, have to wait for the outcome of the tuning experiments regarding HAMOCC parameters. 2) We additionally conducted tuning experiments for a different physical state. These experiments were not planned before 2021, but they yield improved comparison to paleo oceanic biogeochemical records from sediment cores. 3) Together with WP2.3, we additionally implemented prognostic 13CO2 and 14CO2 in the atmospheric component ECHAM. The implementation and testing of this new component for prognostic carbon isotopes took considerable time. This new model component will be used in the next transient deglaciation simulations.

WP2.1 (CAU Kiel)
Due to parental leave during the first four months of this reporting year (from October 2020 until April 2021), the postdoc hired on PalMod has only recently started to work on the PalMod simulations planned for 2021. This delay was foreseeable for some time ahead, and we therefore (as much as possible) internally moved the computation time to other groups that were ready to use it in early 2021, planning to use more computation time in WP2.1 towards the end of 2021 to catch up with the work plan.

Report 2021

WP 2.1 “Marine carbon cycle“, CAU Kiel

As mentioned above, due to parental leave, we have only just started to work on the 2021 simulations.

First, we updated our model version with ballasting to allow a comparison of our simulations to recent PI and LGM model runs with the M4AGO sinking scheme developed at MPI-M. Due to administrative difficulties (CIS account was deactivated; no access to MPI-M's git-repository), this comparison was further delayed, so that no results can be shown yet. However, we are still expecting to finish the comparison as planned by the end of this year.

We are also still expecting to finish one of the two originally planned transient deglaciation experiments with particle ballasting by the end of 2021, ideally with prognostic rather than purely diagnostic CO_2. The simulations with prognostic CO_2 (where HAMOCC 'sees' the interactively calculated pCO_2, and only the radiation in ECHAM is calculated using the prescribed deglacial pCO_2 rise) have only recently become possible after the implementation of prognostic $^{13}CO_2$ and $^{14}CO_2$ in ECHAM and the coupling of air-ocean and air-land fluxes at MPI-M (in collaboration with WP2.3, see report by WP2.1 MPI-M).

WP 2.1 “Marine carbon cycle“, MPI-M

1) HAMOCC tuning for pre-industrial states

We conducted a series of time-slice experiments to improve the model-observation comparison for the pre-industrial ocean. Specifically, we have improved the representation of iron limitation in Southern Ocean (see Fig. 1; previously the model only simulates iron limitation south of 55oS, not shown). We have also improved the representation of organic matter export. Figure 2 shows the model well captures the export efficiency (the ratio of organic matter flux at 1000 m to the flux at 100 m).

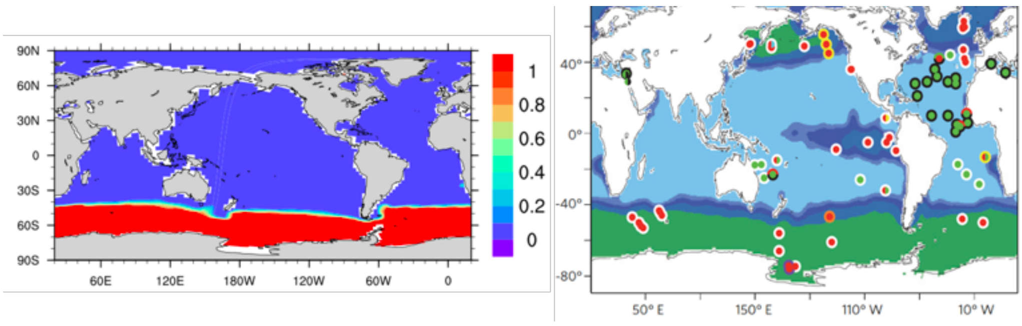

Figure 1: The simulated iron limitation (indicated by value 1 in the left panel) and the observed iron limitation (red colour in the right panel; Moore et al., 2013).

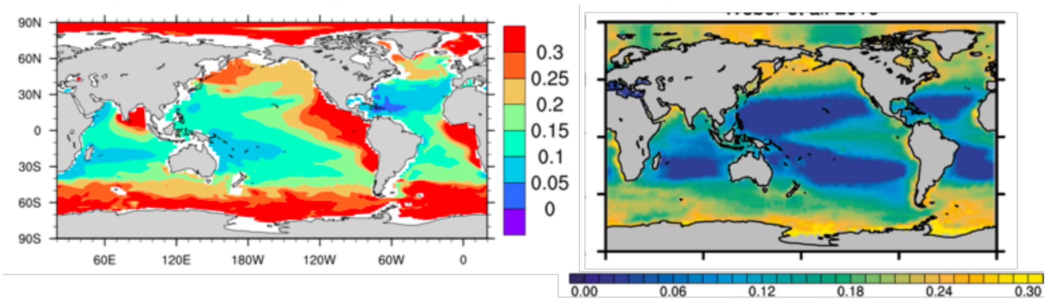

Figure 2: Transfer efficiency in the model (left panel) and of the observation-based estimate from

Weber et al. (2016).

2) Sensitivity study for MPIOM tuning

The default paleo version of MPI-ESM (model parameters tuned by WG1) features an LGM with a greater strength and deeper boundary between the NADW and AABW cell than the pre-industrial state. Such a strongly ventilated LGM ocean in the model yields poor comparison to δ13C sediment core records. We found a weaker background vertical mixing in MPIOM produces a weaker and shallower LGM AMOC than pre-industrial. This LGM AMOC state now captures the main features of the δ13C paleo data (see Fig. 3).

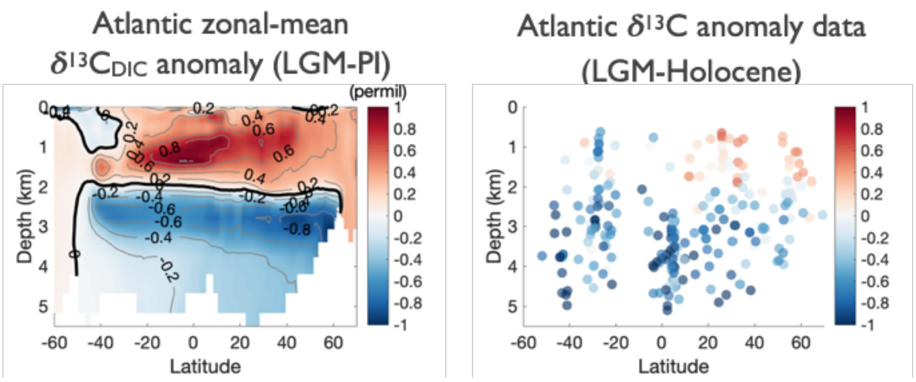

Figure 3: Comparison of simulated δ13C anomaly to paleo data (Peterson et al. 2014) in the Atlantic Ocean.

3) Further model development

In 2021 we further carried out two model developments. The first is to implement the prognostic 13CO2 and 14CO2 in ECHAM and the coupling of air-ocean and air-land fluxes. This work is done in collaboration with WP2.3. Current we are testing this new model component. The second development is to incorporate an advanced aggregate sinking scheme M4AGO (Maerz et al. 2019). Previously the M4AGO scheme was only tuned for low resolution MPI-ESM. When applied to the paleo version of MPI-ESM, which uses a coarse resolution set-up, some large model biases occur regarding the ocean biogeochemical parameters. Thus, we are currently tuning the model parameters of the M4AGO scheme.

WP2.2 "Terrestrial Carbon Cycle", MPI-M

For 2021, WP2.2 had planned to work on the glacial inception and the consequences of lowering sea level, as well as working on the carbon storage in peatlands.

These experiments are still planned for the second half of 2021, but in the first half of 2021 we focused on a question left over from 2020, the mismatch in vegetation development between proxy data and models.

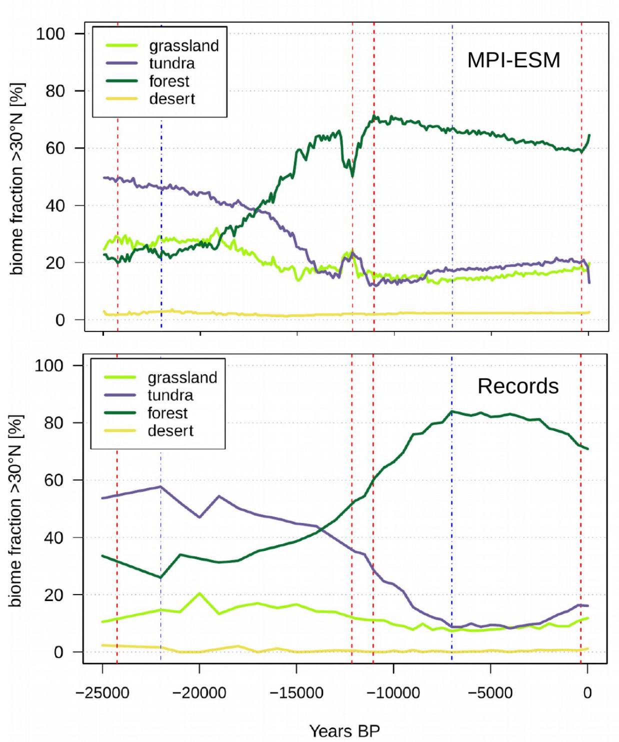

Figure 4: (Top) Biomes as assessed from MPI-ESM plant functional types, (Bottom) Biomes as reconstructed from Pollen data (areas north of 30°N).

Fig. 4 shows the vegetation cover, expressed as biome coverage, as diagnosed from MPI-ESM in the top half, while the bottom half shows the biome coverage as diagnosed from pollen records (similar figure shown in last year's report). One striking difference is that tree cover develops much faster in the model than in the reconstructions.

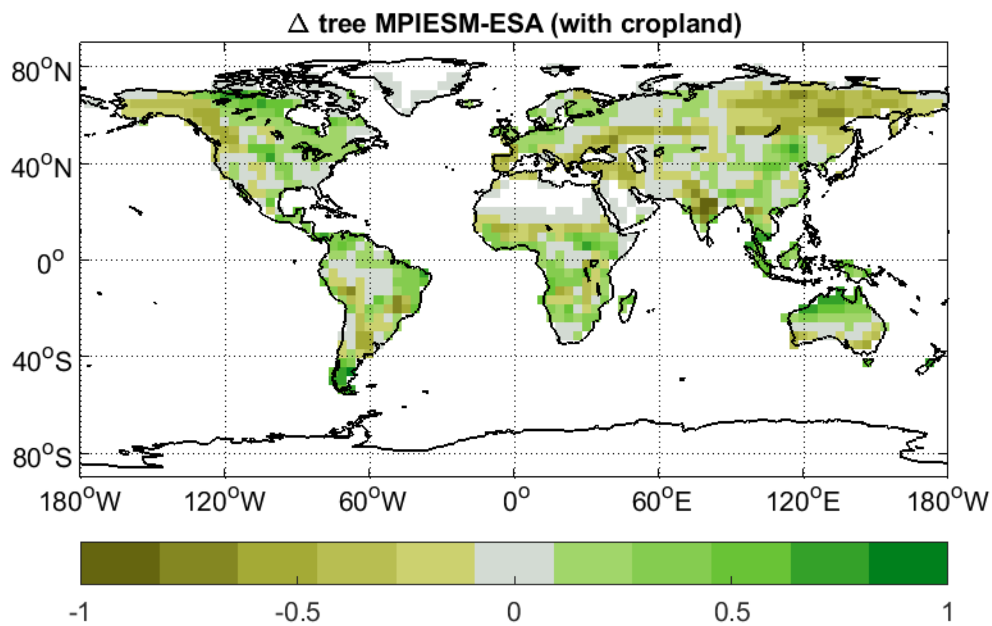

Figure 5: Difference in MPIESM tree cover to ESA CCI land cover data set

We therefore re-evaluated the vegetation parametrisation in MPIESM in order to improve the tree cover in the model. In comparison to the present-day land cover data set ESA-CCI (Fig. 5), significant decreases in tree cover in Eastern Siberia and southern Alaska are apparent, as well as in western Eurasia around 40°N. While not all of these mismatches can be improved by changing model parameters, some can. We have also developed a number of hypotheses on causes for the temporal mismatch, which is only partially related to the spatial mismatch – hypothesis testing experiments are running on Mistral presently, but aren't yet finished.

WP 2.3 "Methane cycle" (MPI-M)

In 2021, we finalised the publication on future methane concentrations we had reported on in the 2020 report (Kleinen et al., 2021a), with data published in the DKRZ LTA (Kleinen et al., 2021b). The publication should be available by the time the report is received by DKRZ.

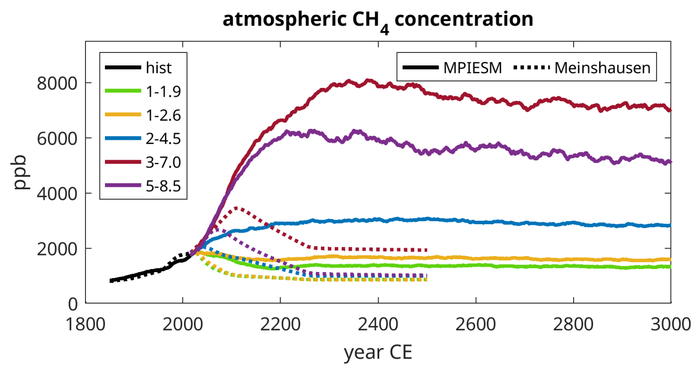

Figure 6: Atmospheric CH4 concentration in scenario experiments with MPIESM (solid lines), compared to Meinshausen et al. (2020) CMIP6 scenario data.

Results, shown in Fig. 6, are striking in that future CH_4 is apparently grossly underestimated in the Meinshausen et al. (2020) scenarios employed in the CMIP6 exercise. This underestimate is due to the fact that previous authors assumed that anthropogenic emissions of CH_4 are dominating the methane cycle and that the natural emissions of CH_4 would not change under future climate conditions. We could, however, show that natural emissions are highly dependent on temperature and atmospheric CO_2, leading to much larger emissions under future (warmer) climate conditions.

Furthermore, we worked on improving the CH_4 sink parameterisation in MPIESM. While our previous formulation only considered Lightning NOx and its influence on the CH_4 lifetime, we now also consider further sources of reactive carbon (RC) and reactive nitrogen (RN). Briefly, RC tends to prolong the lifetime of CH_4 in the atmosphere, while RN tends to shorten it.

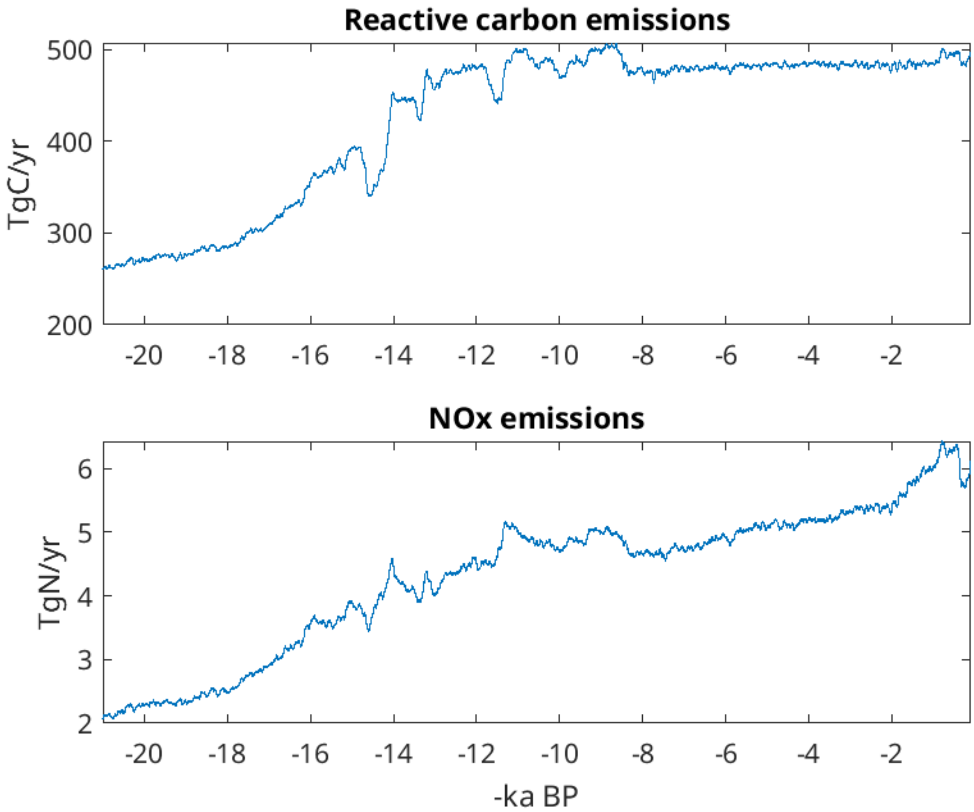

Figure 7: Emissions of reactive carbon (RC, top) and NOx (bottom) from the terrestrial biosphere**.**

As a result of these changes in terrestrial emissions of trace gases, the atmospheric lifetime of methane becomes more variable, leading to increased lifetimes during the Holocene in comparison to the glacial. The envisioned publication covering the transient evolution of CH_4 during the deglaciation, however, will require one final experiment, to be performed later in 2021, due to a bug in the coupling of ECHAM6 and MPIOM found during ICON development.

WP 2.3 “Methane cycle” (MPI-C)

Within the reported 2020–2021 period, we have continued numerical experiments on atmospheric physicochemical state variations using comprehensive “unified” setup of the EMAC model, which includes detailed representation of the gas-phase kinetic chemistry (including air O2 clumped isotope composition), treatment of aerosol/dust interactions and on-line trace-gas emission sub-models. The simulated experiments, commonly tackling variations in methane lifetime and atmospheric oxidative capacity in general, were targeted to gauge further in detail (1) the effects of CH4 burden changes, (2) the effects of tropospheric dust load increase, and (3) the applicability of clumped O_2 isotope composition as a proxy for atmospheric oxidative capacity.

Regarding (1), increased CH_4 burden (*B*) leads to greater competition for hydroxyl radicals (OH, the major removal agent for methane) thus implicitly leading to additional (i.e. not caused by mere growth of CH_4 abundance) increase of methane lifetime (τCH4). Such so-called “self-feedback” effect is often quantified using the scant formulation (e.g., Wild and Prather, 2000) under the assumption that other factors affecting atmospheric physicochemical state (e.g. emission fluxes of other trace gases or climate variations) do not change. In the range of sensitivity experiments, we have simulated doubled and quadrupled CH_4 burden in both the PD and LGM conditions. The obtained changes to τCH4 showed discernible sensitivity s of lifetime *vs.* burden changes ($s = \partial\ln(\tau CH4)/\partial\ln(B)$) varying between 0.20 and 0.32, with higher values characteristic for PD conditions and in line with earlier findings (e.g. Voulgarakis *et al.*, 2013). Ultimately, however, the “perturbation” formulation does not provide means of predicting the value of s for particular climate/boundary conditions, except performing a dedicated simulation with an AC-GCM. In contrast, the CH_4 lifetime changes in our experiments are adequately predicted by the τCH4 fit currently being used in transient simulations with MPI-ESM (see Figure 8 yellow symbols). Another important result of the sensitivity simulations with increased CH4 burden is the perceptible effect on tropospheric ozone (O3) abundance, which increases by up to 50% (PD conditions, quadrupled B) due to enhanced production via CH4 oxidation chain intermediates involving hydrogen and nitrogen oxides (HOx and NOx) species cycles. Such is an important finding for future projections of atmospheric state and ensuing effects for biosphere.

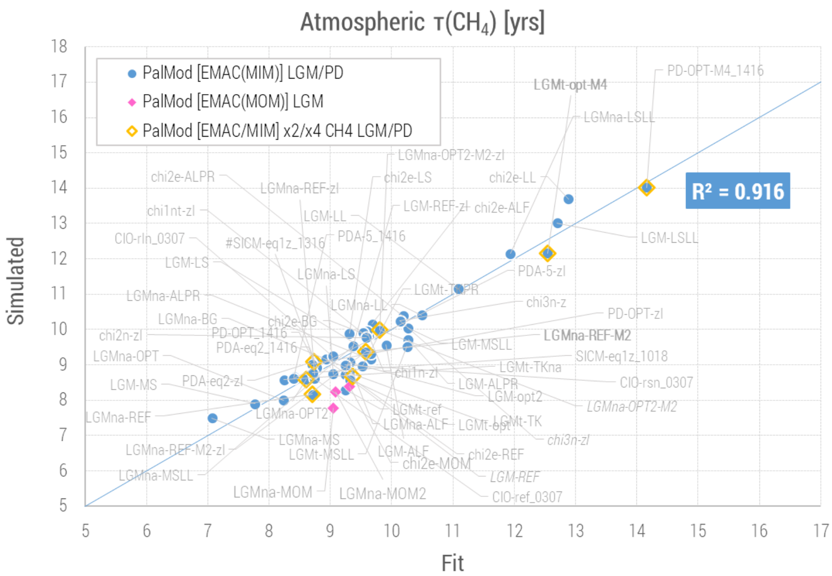

Figure 8. Fitted (abscissa) vs. simulated (ordinate) atmospheric CH4 lifetime obtained in experiments with EMAC (updated lifetime fit parameterisation using NOX as the RN parameter). Yellow symbols denote the experiments with doubled and quadrupled CH4 burden (both LGM and PD conditions).

The potential of atmospheric dust load in modulating atmospheric oxidative capacity (2) was estimated in the LGM conditions experiments. The PMIP3 protocol followed in our model setup prescribes the use of PI or PD dust loading for LGM, partly due to absence of more reliable estimates. Nevertheless, dust deposition fluxes around 21ka are gauged to be substantially larger than that in PD (e.g. factor 5–12 in Antarctica, data from Lambert *et al.*, 2012). We have probed from doubling to octupling of tropospheric dust loading (whilst keeping the relative vertical distribution of dust unchanged) in sensitivity experiments, which results in opposite changes to *τ*CH4 in lower and upper troposphere which superpose as total minor tropospheric effect. Such is the result of vertical redistribution of the photolysis reaction rates, which decrease close to the surface due to reduced solar flux and increase in the upper troposphere due to augmented backscatter from lower layers (other indirect effects such as changes in cloud formation are negligible). The largest effect (from octupling of dust burden) obtained at 1.3% and 4.4% increase in tropospheric and stratosphere O_3 photolysis rates, with the concomitant increase in atmospheric CH_4 lifetime or mere 2.7% (comparable to simulated interannual variation in *τ*CH4). We therefore conclude that dust load variations play a minor role in determining atmospheric oxidative capacity and do not need to be accounted for in CH_4 lifetime parameterisation at the current stage.

Finally, we have completed and analysed the experiments on clumped O_2 isotopes variations in the PD and LGM conditions (3). The overarching goal of these were to confirm whether air O_2 clumped isotope signature (denoted Δ36) may be used as a proxy for tropospheric temperature and O_3 burden variations. The issue is that Δ_{36} signature is constantly transported and mixed in the atmosphere, whereas slow resetting of its value occurs in the lower troposphere (bringing lower Δ_{36} values indicative for higher temperatures), and intensive photo-chemistry in the upper troposphere/lower stratosphere counteracts with resulting higher Δ_{36} values (lower temperatures, higher O_3 abundances). Ultimately, Δ_{36} values at the surface (i.e. where they get trapped in ice cores) is a convoluted result of these processes, with about one half of variations reflecting changing conditions in the troposphere. Although present day conceptual understanding of Δ_{36} distribution may still be not complete due to yet unidentified complex isotope effect(s) in O3 photochemistry, simulations with EMAC predict consistent changes of the Δ_{36} signature with changing tropospheric ozone burden (probed in three sensitivity simulations in each time-slice) and temperature. This is exemplified in Figure. 9 which shows simulated Δ_{36} at the EGRIP site location as a function of tropospheric ozone burden in the LGM and PD conditions. We note that for the LGM, nearly linear O_3−Δ_{36} relationship is obtained, with higher sensitivity due to much less reactive nitrogen surface emissions (RN) and resulting tropospheric burden of NOx in natural (preindustrial) atmospheres. Also, only about one-half of the PD vs. LGM difference in Δ_{36} values are attributable to changes in tropospheric temperature; the remaining changes are due to modified vertical distribution of ozone and NOx, whose abundance in lower troposphere is much larger due to large anthropogenic RN component. Ultimately, for each climate state we can obtain a specific O3−Δ_{36} “calibration” curve and hence link Δ_{36} to past tropospheric oxidative states, provided that temperature distribution and transport/mixing processes in the troposphere are adequately accounted for. Therefore, with the help of AC-GCMs we can interpret past atmospheric physicochemical state via Δ_{36} ice core records that recently became available.

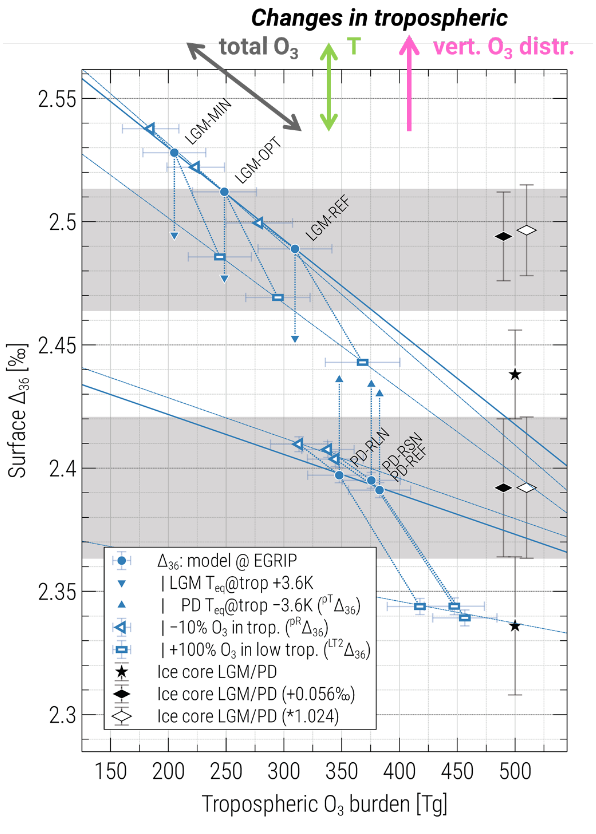

Figure. 9. Air O_2 clumped isotope composition (Δ_{36}) as a function tropospheric ozone burden obtained in EMAC experiments for the present-day and LGM conditions. at the EGRIP site (filled circles). Other blue-colored symbols denote sensitivities of Δ_{36} signature to various processes involved (changes in tropospheric temperature, O_3 vertical distribution). Black symbols denote the preliminary (uncalibrated) data from the EGRIP ice core (kindly provided by T. Röckmann, IMAU, pers. comm.)

Error! Bookmark not defined.Error! Bookmark not defined.Error! Bookmark not defined.Error! Bookmark not defined.Error! Bookmark not defined.Error! Bookmark not defined.Error! Bookmark not defined.Error! Bookmark not defined.Error! Bookmark not defined.Error! Bookmark not defined.Error! Bookmark not defined.Error! Bookmark not defined.Error! Bookmark not defined.Error! Bookmark not defined.Error! Bookmark not defined.Error! Bookmark not defined.NOx**Error! Bookmark not defined.Error! Bookmark not defined.Error! Bookmark not defined.**NOxCH4**Error! Bookmark not defined.**OHO3OHCH4OHOH**Error! Bookmark not defined.Error! Bookmark not defined.Error! Bookmark not defined.Error! Bookmark not defined.**OH**Error! Bookmark not defined.Error! Bookmark not defined.**O3**Error! Bookmark not defined.Error! Bookmark not defined.**

2.2 Publications and references

Publications derived from bm1030

Kleinen, T., Gromov, S., Steil, B., and Brovkin, B.: Atmospheric methane underestimated in future climate projections. *Environmental Research Letters*, accepted, 2021a.

Kleinen, T., Gromov, S., Steil, B., and Brovkin, B.: Natural methane emissions 1850-3009. *World Data Center for Climate (WDCC) at DKRZ,* http://cera-www.dkrz.de/WDCC/ui/Compact.jsp?acronym=DKRZ_LTA_060_ds00007, 2021b.

Liu, B., Six, K. D., and Ilyina, T.: Incorporating the stable carbon isotope 13C in the ocean biogeochemical component of the Max Planck Institute Earth System Model, *Biogeosciences*, 18, 4389–4429, doi:10.5194/bg-18-4389-2021, 2021.

References:

Dallmeyer, A. e*t al.*: Harmonising plant functional type distributions for evaluating Earth System Models. *Climate of the Past*, *15*, 335-366, 2019.

Maerz, J., Six, K. D., Stemmler, I., Ahmerkamp, S., & Ilyina, T.: Microstructure and composition of marine aggregates as co-determinants for vertical particulate organic carbon transfer in the global ocean. Biogeosciences, 1–55. http://doi.org/10.5194/bg-2019-378, 2019.

Kleinen, T. *et al.*: Terrestrial methane emissions from the Last Glacial Maximum to the preindustrial period. *Climate of the Past*, 16(2):575–595, 2020.

Meinshausen, M. *et al.*: The shared socio-economic pathway (SSP) greenhouse gas concentrations and their extensions to 2500. *Geoscientific Model Development*, 13(8):3571–3605, 2020.

Lambert, F. *et al.*: Centennial mineral dust variability in high-resolution ice core data from Dome C, Antarctica, Clim Past, 8, 609−623, doi: 10.5194/cp-8-609-2012, 2012.

Moore, C. M., Mills, M. M., Arrigo, K. R., Berman-Frank, I., Bopp, L., Boyd, P. W., Galbraith, E. D., Geider, R. J., Guieu, C., Jaccard, S. L., Jickells, T. D., La Roche, J., Lenton, T. M., Mahowald, N. M., Marañón, E., Marinov, I., Moore, J. K., Nakatsuka, T., Oschlies, A., Saito, M. A., Thingstad, T. F., Tsuda, A., and Ulloa, O.: Processes and patterns of oceanic nutrient limitation, Nat. Geosci., 6, 701–710, https://doi.org/10.1038/ngeo1765, 2013.

Peterson, C. D., L. E. Lisiecki, and J. V. Stern: Deglacial whole-ocean δ13C change estimated from 480 benthic foraminiferal records, Paleoceanography, 29, 549–563, doi:10.1002/2013PA002552, 2014.

Voulgarakis, A. *et al.*: Analysis of present day and future OH and methane lifetime in the ACCMIP simulations, Atmos. Chem. Phys., 13, 2563−2587, doi: 10.5194/acp-13-2563-2013, 2013.

Weber, T., Cram, J. A., Leung, S. W., DeVries, T., and Deutsch, C.: Deep ocean nutrients imply large latitudinal variation in particle transfer efficiency, P. Natl. Acad. Sci. USA, 113, 8606–8611, 2016.

Wild, O. and Prather, M. J.: Excitation of the primary tropospheric chemical mode in a global three-dimensional model, J. Geophys. Res. Atm., 105, 24647−24660, doi: 10.1029/2000JD900399, 2000.

3. Project 1029 / WG3

Project title: PalMod WG3 -Datasynthesis
Project lead: M.Werner (AWI)
Subproject lead: T.Läpple (AWI), A.Paul (MARUM)
Allocation period: 01.01.2021 – 31.07.2021

3.1 Report on resources used in 2021

Our sub-project WP3.3-TP2 has been granted 151,200 node hours for the year 2021.

The resources were applied for climate simulations using AWI-ESM-wiso, an AWI-ESM model version enhanced by stable water isotope diagnostics, for several time intervals. These intervals included (1) the pre-industrial, (2) mid-Holocene, (3) last glacial maximum (LGM), and (4) abrupt transitions during the deglacial time period. During the first half year of the report period, we have upgraded the ocean module (FESOM) of AWI-ESM 2.1, to include recent important code improvements of FESOM: a new mixing scheme for the sea water column, updated parameters for sea ice and oceanic processes, the addition of the ICEPACK sea ice thermodynamics package and the implementation of a non-linear free surface mode of the vertical discretization scheme within FESOM. This new scheme allows the total sea water volume to change with time and space, which is very relevant for more realistic paleoclimate simulations on glacial-interglacial time intervals. Moreover, we have improved the formulation describing isotope tracers over sea ice. Due to these different updates of the FESOM model, we had to performed several test simulations under pre-industrial climate conditions using the various new physical parameters and code updates of the model. This additional tuning process, which has been finished now, was unforeseen when we applied for computing resources for 2021. It consumed about 50% of the computing resources of the first half of 2021 and delayed the progress of the planned paleoclimate simulations for several months.

Since our project aims to simulate the last glacial-interglacial transition, a good LGM (last glacial maximum) state is very crucial, as it serves as a starting point for the transient simulation. The greenhouse gas concentrations and the orbital parameters are well known for LGM as required model boundary conditions. But the glacial LGM topography, several different reconstructions, e.g., ICE6G and GLAC1D, exist. Our isotope-enabled LGM simulations allow a direct comparison with various proxy records to evaluate the effect of the different prescribed ice sheets. Our first LGM simulation results showed modeled deltaO18 in precipitation over Greenland, which was much less depleted in our simulations as compared to various ice core data. Therefore, in order to find better boundary conditions for our LGM simulation, we performed several additional LGM runs based on the different ice sheet topography reconstructions and variations in some isotope parametrizations, which used about 23000 node hours.

The remaining resources in 2021 will be used for finalizing the ongoing pre-industrial and LGM simulations (the deep ocean has not reached isotope equilibrium, yet), as well as a new transient run for the mid- and late-Holocene. In cooperation with the physical modelling of WG1 we will also start working on the proposed transient simulations of the last deglaciation and the last inception.

3.2. Short summary of achieved results

3.2.1 Pre-industrial climate

We took advantage of the most recent release of AWI-ESM with the novel nonlinear free surface formulation, and here we show some results of our pre-industrial control simulation.

Fig. 1 presents the temperature at the sea surface and 2-m air temperature over continents. The area-weighted mean global surface temperature (GST) in our pre-industrial simulation is 14.2°C, in good agreement with the estimated global surface temperature for 1951-1980 by NASA GISS (approx. 14 °C).

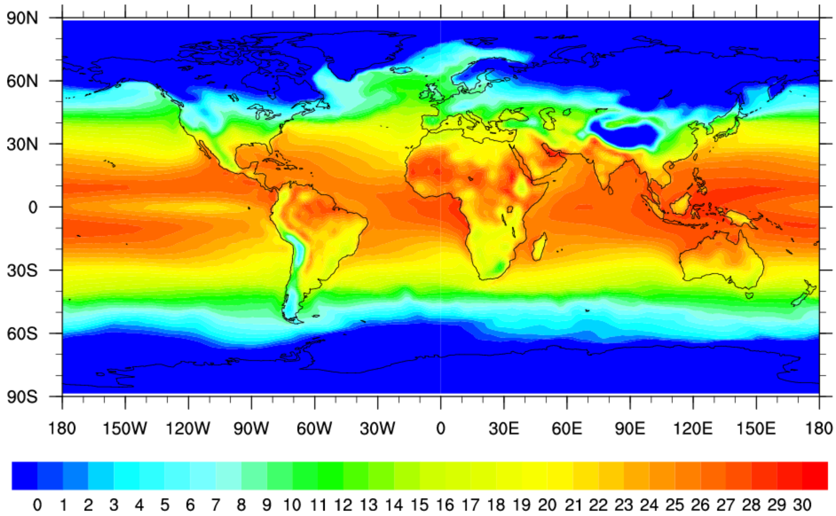

Figure 1. AWI-ESM PI climate simulation: distribution of global surface temperature (units: °C).

The sea ice concentration distribution as simulated in our pre-industrial experiment (Fig. 2) is also comparable with recent observations from National Snow and Ice Data Center (NSIDC) for both Arctic and Southern Ocean, though overestimated in some specific regions like the subpolar Pacific section. However, considering that the pre-industrial climate was a bit colder than the present one, such model-data bias is reasonable.

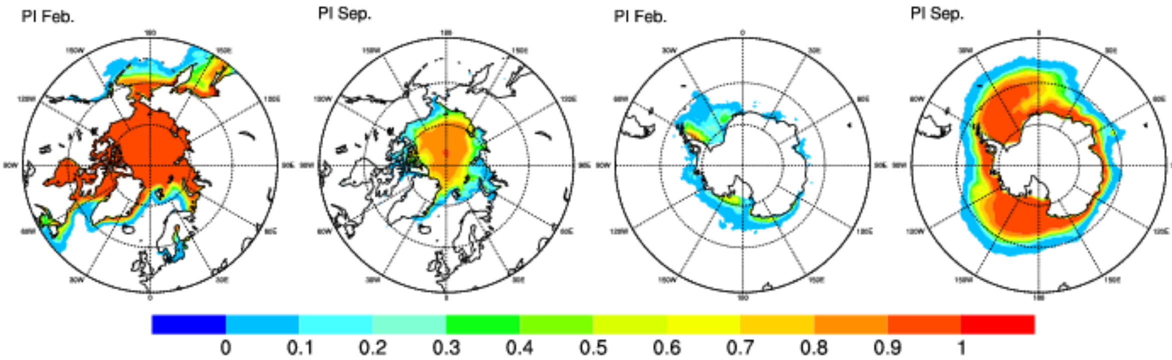

Figure 2: AWI-ESM PI climate simulation: distribution of sea ice concentration (units: grid fraction).

3.2.2 LGM temperature anomalies

As explained above, several isotope-enabled AWI-ESM simulations have been exploited with respect to the LGM climate. Our analyses included an older LGM simulation (published in Kageyama et al., ClimPast, 2020, named “AWIESM1” in Fig. 3), a switch to the finite-volume version of FESOM (simulation “alpha”), an update of the isotope code from ECHAM6.3.04 to ECHAM6.3.05 (“beta”), and the implementation of the non-linear free surface mode within FESOM (“gamma”). For the simulations “AWIESM1”, “alpha” and “beta”, we prescribed the LGM ice sheets based on the ICE6G reconstruction. For the “gamma” setup, two LGM simulations were conducted with different topography applied (i.e., ICE6G and GLAC1D). Fig. 3 shows a comprehensive comparison of the simulated LGM temperature anomalies as compared to the pre-industrial climate for all model versions. A common feature shared by all simulations is the overall colder-than-present LGM climate. Cooling is the most pronounced over the Laurentide ice sheet and the Fennoscandia ice sheet, with a maximum temperature change of -30 K in all model versions. However, the simulated cooling over Greenland and Antarctica has different magnitudes for the different simulations. “AWIESM1” shows the most pronounced cooling over Greenland as compared to the other simulations, which is in better agreement with the reconstructed ice core records. The “alpha” and “beta” simulations show a less pronounced cooling over Greenland as compared to “AWIESM1”. The “gamma” simulations present a strong warming bias over Greenland and its adjacent oceans, especially the Baffin Bay, with either ICE6G or GLAC1D ice sheets applied. For the Antarctic continent, all simulations except “gamma” with the GLAC1D ice reconstruction show a significant cooling, with the maximum anomalies being -25 K over western Antarctica. For “gamma” prescribing GLAC1D ice sheers the cooling over Antarctica is much less pronounced (up to -15 K). This difference between the two “gamma” simulations is due to the much lower LGM Antarctic ice sheet elevation in GLAC1D as compared to ICE6G.

For the next upcoming simulations, we will mainly focus on the model setup used for the “gamma” simulation as this setup employs the option of a full free ocean surface. We will further investigate potential improvements of the boundary conditions for LGM and try to resolve the warm model bias over Greenland, as this leads to the large deviation of simulated isotope values in precipitation.

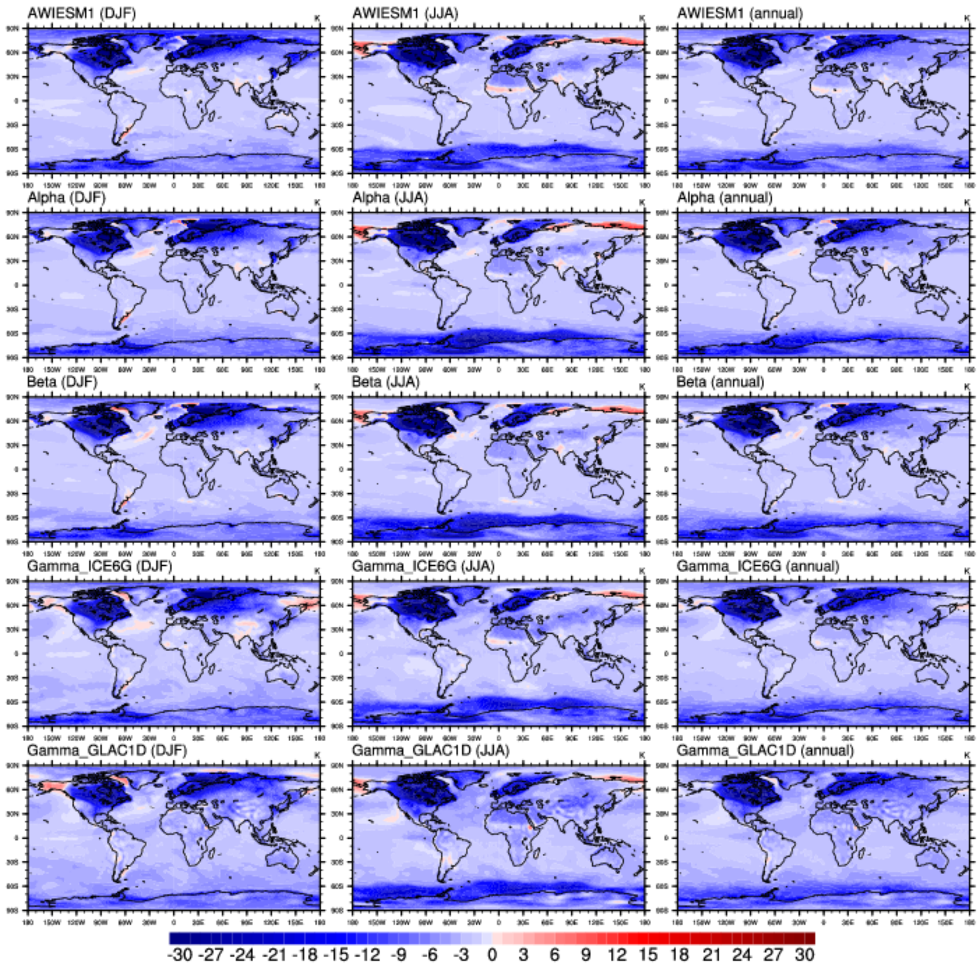

Figure 3: Temperature anomalies (LGM-PI) for several AWI-ESM model configurations (units: K).

3.2.3 Stable Water Isotopes

We updated all AWI-ESM-wiso routines to latest version of AWI-ESM including the option of a non-linear free surface for the ocean model. In addition, we improved the water isotope diagnostics to allow a more realistic simulation of isotope changes in sea ice. Now, during the melting of sea ice and the snow lying on the sea ice, it is explicitly assumed that no isotopic fractionation occurs. Thus, the meltwater contains the same isotopic ratio as its source, either the sea ice itself or the snow lying on top of the ice. On the other hand, equilibrium fractionation occurs during the growth of sea ice and is now also explicitly simulated in AWI-ESM-wiso. For this fractionation process, the most current literature values of the corresponding fractionation coefficients are now used.

As indicated in Fig. 4a, the simulated global pattern of $\delta^{18}O$ in precipitation shows all characteristic patterns in agreement with present-day observations (e.g., latitudinal gradients between subtropics and high latitudes, continental gradients over Eurasia and North America, strong isotope depletion over Greenland and Antarctica). There is a very good agreement between modeled and observed $\delta^{18}O$ values. Fig. 4b presents the global distribution of simulated annual mean δO18 values in ocean surface waters under PI conditions. The latitudinal gradients between subtropics and high latitudes, isotope enrichment in the North Atlantic Ocean, isotope depletion in the Arctic Ocean and the Antarctic Circumpolar Current region are very well captured by our model. Again, we see a good match between modeled $\delta^{18}O$ values and observations.

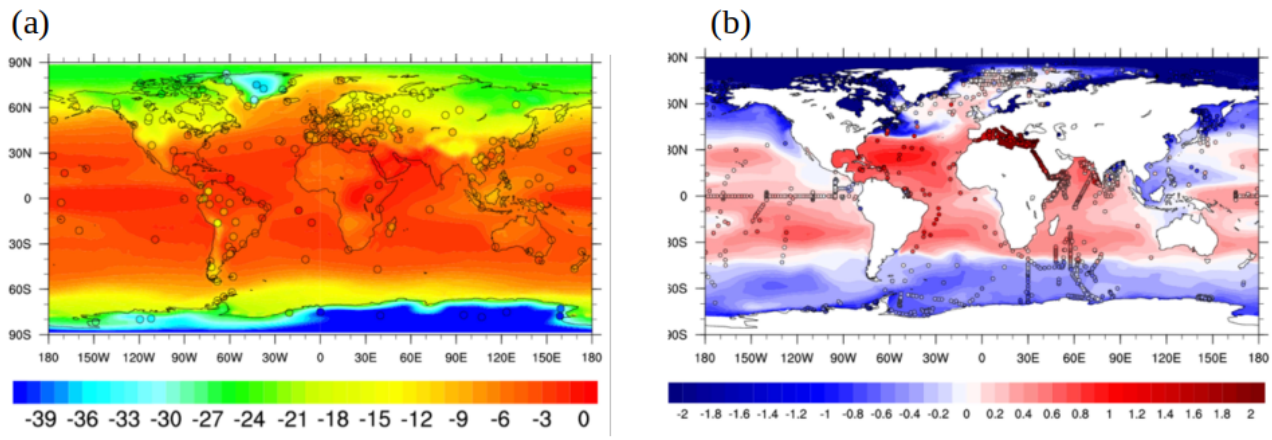

Figure 4: (a) Global distribution of simulated annual mean $\delta^{18}O$ in precipitation under PI conditions. The circles show observed modern $\delta^{18}O$ values in precipitation from the GNIP database and a compilation of ice core data. (b) Global distribution of simulated annual mean $\delta^{18}O$ values in ocean surface waters under PI conditions. The circles show observed modern $\delta^{18}O$ values in sea surface waters from the NASA GISS $\delta^{18}O$ compilation. (Units in both plots: ‰)

Fig. 5a shows a scatter plot of modeled vs. reconstructed anomalies in annual-mean $\delta^{18}O$ in precipitation (LGM-PI), for prescribed ICE6G ice sheets. We find that AWIESM-wiso has a good performance on simulating the change in $\delta^{18}O$ in precipitation over locations of the sub-tropical speleothems as well as Antarctic ice cores. However, large deviations can be found when comparing the modeled results with records from the Greenland ice cores, which is most-likely partly due to the warm model bias over Greenland in the LGM simulation (see above). To further investigate this problem, we applied the GLAC1D ice sheets in a second LGM simulation. As GLAC1D has a much lower mean elevation of the Laurentide ice sheet as compared to ICE6G, the North Atlantic westerly jet is expected to be much weaker, which should lead to a decline in the Atlantic meridional overturning circulation (AMOC) and a colder climate over Greenland. As indicated in Fig. 5b, first analyses from the GLAC1D simulation do not show an improvement but even a worse model-data mismatch for Antarctica and Greenland. This result is somewhat unforeseen and we need to spend some more time on the analysis of this LGM simulation to improve this $\delta^{18}O$ mismatch over Greenland

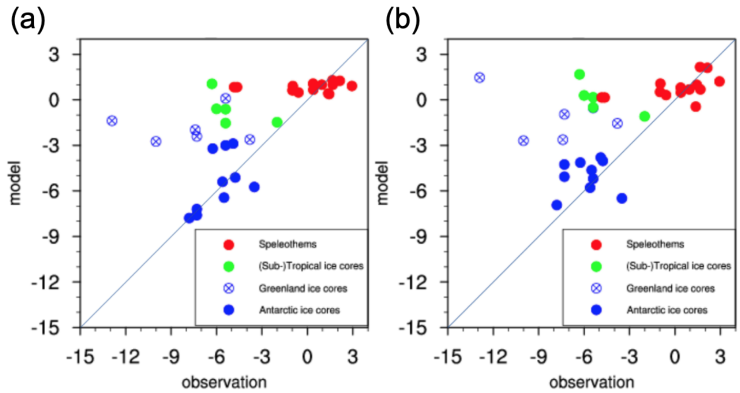

Figure 5: Anomaly of annual-mean $\delta^{18}O$ in precipitation (LGM-PI) compared to ice-core and speleothem data for (a) a prescribed ICE6G ice sheet reconstruction, (b) a prescribed GLAC1D ice sheet reconstruction. (Units in both plots: ‰)

3.3. Future plan

The remaining time in 2021 will be used for finalizing the ongoing PI and LGM simulations (the deep ocean has not reached isotope equilibrium, yet), as well as a new transient run for the mid- and late-Holocene. In cooperation with the physical modelling of WG1 we will also start working on the proposed transient simulations of the last deglaciation and the last inception.

For 2022, details of our workplan are described in the computing resources application request.

4. Project 993 / CC1

Project title: PalMod CC: Cross-cutting activities
Project lead: H.Bockelmann (DKRZ)
Subproject lead: T.Slawig (Uni Kiel), R. Winkelmann (PIK), K.Rehfeld (Uni Heidelberg), O.Bothe(Hereon), A.Hense(Uni Bonn)
Allocation period: 01.01.2021 – 31.07.2021

4.1 Report on resources used in 2021

WP CC.1 / SP1: Enabling high throughput for coupled ESMs

As this subproject follows the aim to increase the integration rate of coupled ESMs within PalMod, we used the resources to develop and test several optimisation approaches for the entire model setups used in WG1 and WG2. In particular, we modified the PISM and FESOM2 model to make use of asynchronous execution schemes to increase the parallelism. Implementation of the same approach has also been started for the biogeochemistry components in MPIOM and FESOM2.

Optimised Parallel I/O in PISM

An I/O analysis of PISM ice sheet model as used in experiments of MPI-M and AWI was conducted for various resolution benchmarks and uncovered the negative effect of the output files writing over the yearly throughput of the time loop. It was observed that the influence of I/O increases with the resolution, as expected, and that it has an effect on both the model scaling and throughput.

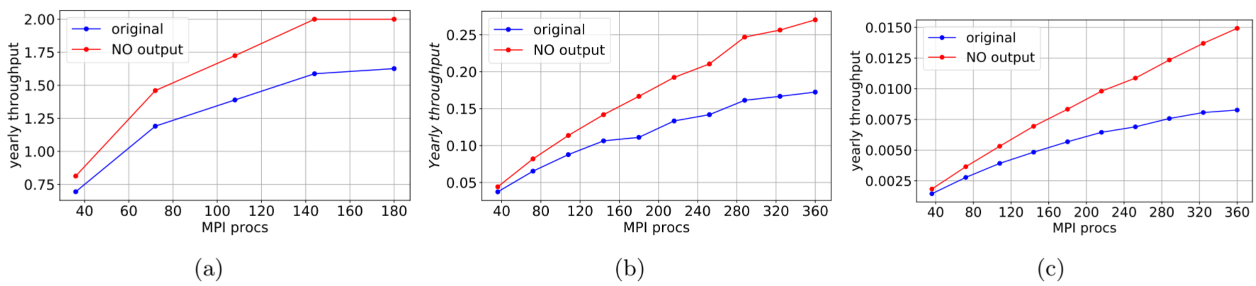

Figure 1: Yearly throughput of original Antarctica set-up and the same set-up without output for 16km (a), 8km (b), and 4km (c) resolution.

The optimisation had the objective to address two main issues that were observed in the performance analysis:

- MPI communication of high number of short messages when not strictly necessary in ocean component
- Improved I/O performance exploiting CDI-PIO library, which allows to exploit asynchronous I/O as it has been already tested in high resolution experiments with ICON.

Figure 2 displays the throughput of the original and the optimised PISM implementation, combining the results from ocean optimisation and CDI-PIO library integration. The results with the original implementation are obtained writing the output files with PNetCDF library. Overall a speedup of more than 2x has been achieved for the low resolution setup used in PalMod.

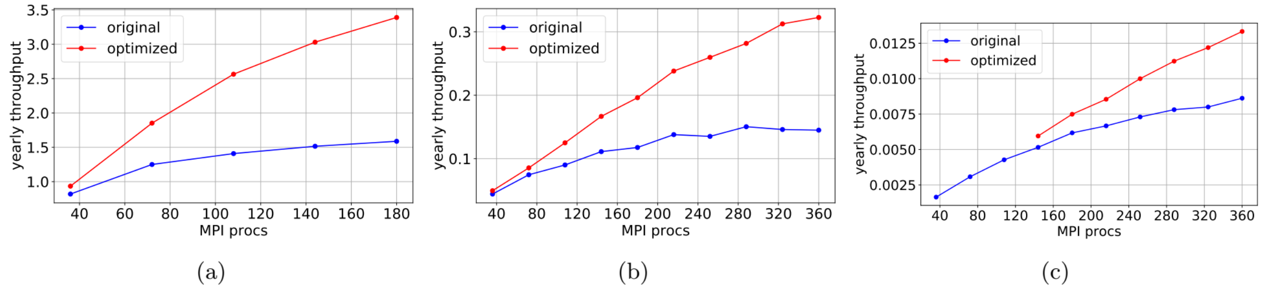

Figure 2: Yearly throughput of original and optimised Antarctica set-up for 16km (a), 8km (b), and 4km (c) resolution.

Optimised Iceberg Model in FESOM2

It has been observed that integrating an iceberg model developed at AWI into FESOM2 increased the runtimes of the fully coupled model more than expected. In addition, it was unclear why the fully coupled model, under almost identical conditions in terms of cores used, hyperthreading usage, compiler and MPI environment selection, runs only about half as fast on the Mistral cluster at DKRZ as on the Ollie cluster at AWI. Therefore, we did a thorough performance analysis and found a severe load imbalance, for which mainly the writing of the restart file in the iceberg model was responsible. In cooperation with AWI, the main part of the restart file handling could be moved from inside the iceberg model, i.e. from the loop iterating over all time steps, to the post processing step in FESOM2. The restart file handling for the remaining parts has also been improved. With these modifications, speedups are achieved, which are comparable to those achieved with the artificial suppression of the restart file handling for benchmark purposes. Finally, a small runtime differences of the respective benchmarks on Ollie and Mistral remains, which can be attributed to the different parallel file systems used on the two clusters, as Lustre is known to perform worse than BeeGFS for frequently writing of small data.

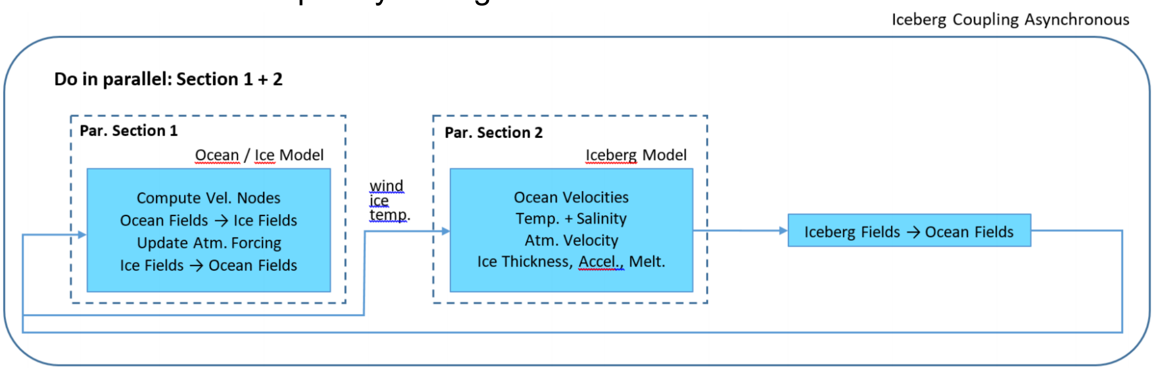

Figure 3: Asynchronous execution scheme of iceberg model in FESOM2.

As a further optimisation, we implemented an asynchronous iceberg coupling in FESOM2 as it became apparent that the standard FESOM2 ocean/ice model and the new iceberg model are rather loosely coupled. Since icebergs move comparatively slowly, in a first step the coupling frequency between FESOM2 and the iceberg model was made variable, so that a data exchange with the iceberg model takes place, for example, only every 2nd, 4th, ... FESOM2 timestep, which immediately improved the runtime without major impact on the iceberg trajectories. In a second step the calculations for the ocean/ice model and the iceberg model can also be performed overlapping in two parallel sections for a speedup of two in best case. For the implementation, we extended the existing MPI parallelization with OpenMP in the sense of a hybrid approach and achieved a speedup of up to 1,6 which is slightly below the theoretically possible value due to a non-optimal implementation of threading capabilities in the MPI library.

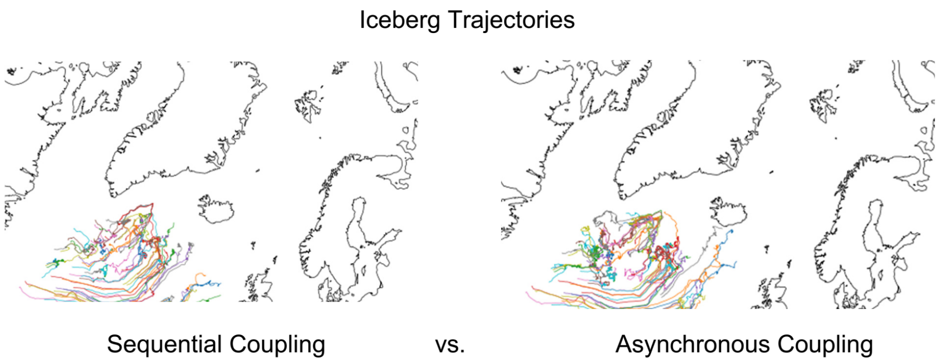

Figure 4: Effects of asynchronous coupling of the iceberg model in FESOM2 on the trajectory of icebergs.

WP CC.1 / SP2: Parallel-in-Time methods for ocean and climate simulations

We were able to stabilize the Parareal algorithm for advection-dominant flow problems modelled by the Burgers' equation, compare Figure 5. Although, the equation does not develop a full turbulent flow, one has to face similar obstacles when it comes to parallelization-in-time algorithms and their complications regarding the non-linear advection term.

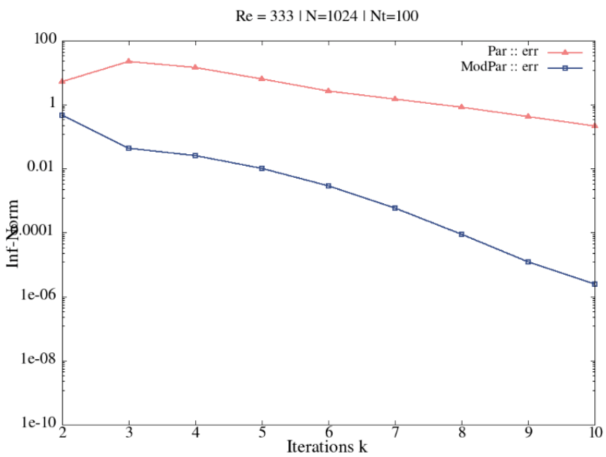

Figure 5: Convergence of the Parareal algorithm for Burgers' equation.

With that being achieved, the standard Parareal algorithm applied to the FESOM2 ocean circulation model has been set up and provided first results. The first configurations considered the lowest resolution (PI mesh, 3140 surface vertices). One of the greatest challenges presents the determination of a best solution to which Parareal is supposed to converge to. After consultation with other working groups and the FESOM developing team we learned, that with finer time steps the computed solutions will become less dissipative. Which is a desirable outcome but demands high computational effort, and hence, advocates the application of Parareal. After investigating the first Parareal runs on the PI mesh, we discovered the well-known behaviour of Parareal for flow problems. In less active regions, like the deep ocean, the algorithm seems to work fine. Closer to the surface, where the advection is dominant, the algorithm stagnates.

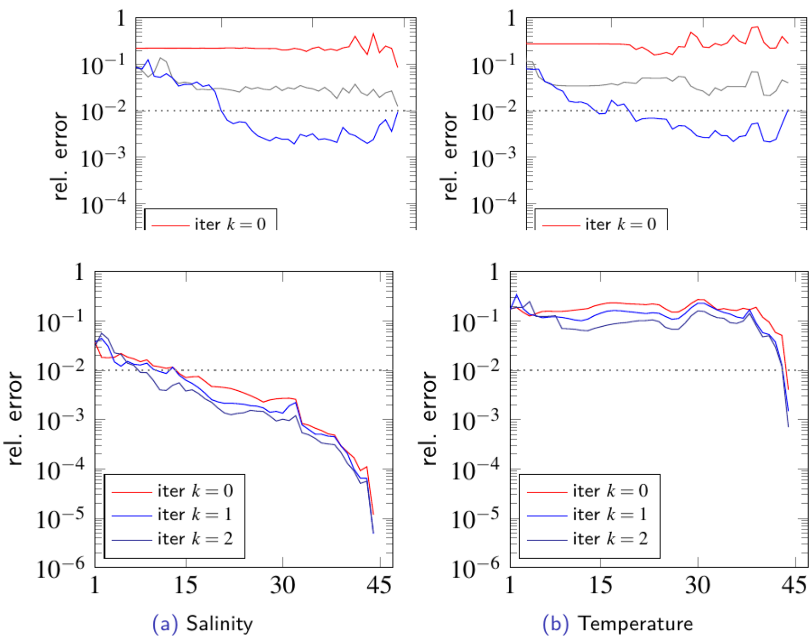

Figure 6: Relative error of the first two Parareal iterations plotted over the ocean depth (0 = surface) at the final simulation time of one year for velocity, temperature and salinity.

If the velocity fields at the ocean's surface are not improving, the tracer for temperature and salinity will stagnate as well. Currently, the modification for advection-dominant problems like Burgers' equation is adapted to Parareal runs with FESOM2 on the PI mesh. Once, the modified algorithm is implemented and validated we proceed to CORE mesh runs in parallel.

WP CC.1 / SP3: Paleo-lakes and hydrology on exposed shelves + land-sea carbon and nutrient transfer related to sea level changes in MPI-ESM

The integration of the standalone prototype of the lake model into the HD model within JSBACH such that the rivers and lakes form a single combined sub-model is now complete and checked for water balance issues. The lake model is now fully integrated into the MPI-ESM1 PalMod transient setup and has been used to simulated 5500 years of lake evolution between 16000YBP and 10500YBP (along with a number of shorter runs for technical tests). A number of technical issues have corrected thanks to the experience gained from making this run and this run will be continued on into the Holocene over the summer. Significant progress has been made on the optimization of tools used by both the dynamic river and dynamic lake scripting to reduce their runtime and thus contribute to increasing to overall model throughput.

The global biogeochemical model HAMOCC has been technically adjusted to take into account the combination of a fully interactive adaptation of the ocean bathymetry, a transient river routing and the land-sea carbon and nutrients exchanges. A publication is in preparation to present the developments and the results during the last deglaciation (between 21-12 ka). Different sensitivity experiments were performed during Meltwater Pulse 1a (MWP1a – between 15-14 ka). They highlight the key role of the terrestrial organic matter inputs to the ocean and especially the wood and humus inputs, on the local CO_2 outgassing to the atmosphere for a few hundred years. The outgassing observed at regional hotspots like in Indonesia is however not enough to affect the global behaviour of the ocean since the land-sea fluxes only represent 3.5% of the Mixed Layer Depth carbon inventory. Sensitivity experiments with modified carbon to nutrients content for terrestrial organic matter inputs, remineralization rate and timescale (parameters that are not well constrained), highlight that a higher carbon to nutrients ratio than the reference deglaciation simulation has no consequences on the CO_2 outgassing during the MWP1a whereas lower values lead to less remineralized terrestrial carbon in the ocean and hence smaller outgassing (Figure 7).

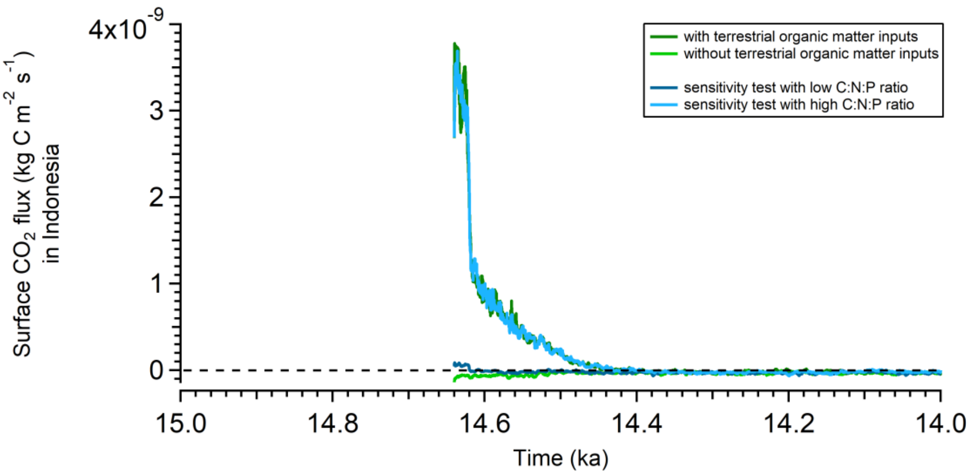

Figure 7: Surface CO_2 flux between the ocean and the atmosphere after a flooding event in Indonesia during MWP1a for the reference deglaciation simulation (dark green), the sensitivity experiment without terrestrial organic matter inputs (light green) and the sensitivity experiments with low (dark blue) and high (light blue) stoichiometry for terrestrial organic matter. Positive values indicate an outgassing to the atmosphere and negative values indicate an up taking by the ocean.

The transient deglaciation simulation has continued to run up to 9.6 ka. A second abrupt meltwater pulse following the melting of the ice sheets happens between 12-11 ka. During this millennial event, coastal areas are flooded and 36.8 GtC of terrestrial organic matter are transferred to the ocean (which is 57% higher than during MWP1a). Most of this terrestrial organic matter inputs comes from Indonesia like during MWP1a, but North-West Africa and central America also contribute with large land-sea fluxes resulting from changes in precipitations and terrestrial biosphere productivity at that time. As a consequence, regional oceanic CO_2 outgassing takes place.

WP CC.1 / SP4: Development of the PICO ice shelf cavity model into a “pop-up” model for use in transient glacial simulation

There was no explicit request for resources at DKRZ but in order to facilitate the cooperation between scientists in the CC.1 work package, some TiB on WORK were allocated for data sharing.

WP CC.2 / SP1 - 4: Data management and model data compariso

The data management and model data comparison toolbox development in PalMod have been shifted to project ID bk1192.

5. Project 1192 / CC2

Project title: PalMod CC2: Datamanagement
Project lead: S.Gehlot (DKRZ)
Subproject lead: K.Peters (DKRZ)
Allocation period: 01.01.2021 – 31.07.2021

5.1 Report on resources used in 2021

A workflow and a recipe detailing the import, access, share and distribute the data via the common data pool supplied by bk1192 is developed (and distributed PalMod-wide) in close collaboration with the scientists with respect to their concrete requirements in the year 2021-2022. Since the first allocation of space bk1192 in early 2021 (105TB available each for /work and /arch), **the PalMod data pool continues to build up and grow in storage with the shared data from project partners** (currently using ~32TB, with more data planned to be shared in summer 2021). The table below lists the current overview of storage of shared data at bk1192.

Overview storage space for the data project bk1192

Working Group/ Work package	Lusture work [GByte]	HPSS arch [GByte]	HPSS docu [GByte]
WG 1/ WP 1.1 (MPI-ESM)	1.500	0	0
WG 1/ WP 1.4 (VILMA)	68	0	0
WG 2/ WP 2.1 (MPI-ESM)	9.100	0	0
WG 2 /WP 2.3 (MPI-ESM)	6.100	0	0
WG 3/ WG 3.2	0.04	0	0
WG 1/ WP 1.1 (MPI-ESM) - v2	14.500	0	0
Total used	31.268	0	0

As the model development/evaluation tasks are progressing throughout the PalMod-II working groups, many sub-sets of final/publishable model data are made available to the PalMod data pool storage for the standardization and ESGF publication workflow development. For the year 2021-22, PalMod subproject CC.2/DataManagement will continue to develop a project-wide strategy for the long-term preservation and accessibility of project data to fulfil the funder requirements and also facilitate data reuse beyond the PalMod consortium and influence the layout of project bk1192.

In addition to supporting the data management activities for PalMod-II, the data pool bk1192 will also act as a platform for building up the prerequisite basis for continuing towards PalMod phase 3. As a primary requirement for PalMod phase-III applications for potential research criteria, the project steering committee proposes that all the work packages from PalMod-II make their model data runs available as a prerequisite to continue extension towards the possible phase-III of the project. **The data pool storage is hence envisioned to grow substantially over the next months/year with data subsets coming from all the PalMod-II modeling work packages.**